Research on Chemical Intermediates (2021) 47:1519–1533
https://doi.org/10.1007/s11164-020-04362-x

Enhanced photocatalytic activity in metal phthalocyanine-sensitized TiO_2 nanorods

Xuefei Zhou[1] · Xiuxiu Wang[1] · Jinxing Li[1] · Xuejun Zhang[1]

Received: 9 September 2020 / Accepted: 11 December 2020 / Published online: 22 January 2021

Abstract

Two novel metal phthalocyanines (Zn Tetra(butylformate-phenoxy)phthalocyanine (ZnTBPP) and Zn Tetra(tert-butyl-phenoxy)phthalocyanine (ZnTTPP)) were synthesized. Besides, TiO_2 nanorods (PN) are prepared through the hydrothermal method. The synthesized metal phthalocyanines are used to sensitize TiO_2 nanoparticles (P25) and PN. Then, four types of metal phthalocyanine-sensitized TiO_2 composite photocatalytic materials (ZnTBPP/P25, ZnTTPP/P25, ZnTBPP/PN and ZnTTPP/PN) are obtained and characterized by methods of X-ray diffraction, scanning electron microscopy, nitrogen adsorption–desorption, Fourier-transform infrared spectroscopy, UV–Vis diffuse reflectance spectroscopy, fluorescence spectra and density-functional theory. At last, the photocatalytic degradation of rhodamine B (RhB) is taken as an example to study the photocatalytic activity of composite photocatalytic materials. The results show that the photocatalytic activity of the composite photocatalytic material is stronger than that of TiO_2. This is because in the photocatalytic process, the loading of metal phthalocyanine can expand the material's photoresponse range and enhance its light absorption performance. At the same time, the metal phthalocyanine can optimize the energy-level structure of the material and reduce the electron–hole recombination. Besides, we found that the photocatalytic activity of nanorods is stronger than that of the nanoparticles because the nanorod structure with a large specific surface area can not only increase metal phthalocyanine load, but also expose more active sites.

Keywords Titanium dioxide nanorods · Metal phthalocyanine · Sensitized · Photocatalytic

Supplementary Information The online version of this article (https://doi.org/10.1007/s11164-020-04362-x) contains supplementary material, which is available to authorized users.

✉ Xuejun Zhang
zhangxuejun@nuc.edu.cn

[1] North University of China, Taiyuan 030051, Shanxi, China

Introduction

The over-exploitation of fossil fuels has brought about increasingly serious problems in energy depletion and environmental pollution [1, 2]. By applying the photocatalysis technology, solar energy can be directly adopted to degrade organic pollutants, which has attracted scientists' attention [3, 4]. Semiconductor photocatalysis technology has the advantages of high efficiency, low energy consumption, simple operation, mild reaction conditions and no secondary pollution. The technology can effectively convert organic pollutants into inorganic molecules [5, 6]. Among various semiconductor photocatalytic materials, TiO_2 gains favor by virtue of its high catalytic activity, well-performed stability, low price and no toxicity to human body. It enjoys great potential in the circle of sewage treatment and air purification [7–9].

The process of pollutant photodegradation can be generally divided into three stages [10, 11]. Firstly, the photocatalytic material captures light energy to obtain energy. Secondly, the photocatalytic material generates electron–holes by electron transition. Finally, electron–holes are harnessed to conduct the redox reaction to degrade organic pollutants [12–15]. There are still some drawbacks for TiO_2 to be applied as a photocatalyst in the photocatalytic degradation of organic pollutants. For example, TiO_2 can only absorb ultraviolet light. It means that TiO_2 can only absorb and utilize 3%~5% of the energy in solar spectrum [16–18]. TiO_2 has a 3.2 eV conduction-valence gap width and requires higher energy to generate electron–holes. A part of the generated electron–holes are used to conduct the redox reaction. The other part are for carrying out the electron–cavity recombination [19–21]. TiO_2 is small in particle size and high in surface energy. Hence, it can easily agglomerate and fail to reach satisfactory specific surface area. Currently, there are many ways to enhance the photocatalytic activity of TiO_2, such as metal mixing [22–24], dye sensitization [25, 26], and preparing lower-dimensional morphology like nanorods, nanotube arrays, nanosheets and so forth [27, 28]. All these studies work to enhance the photocatalytic activity of TiO_2 to some extent. The research on the three stages of photocatalytic process has been conducted to enhance the photocatalytic activity of TiO_2, based on the defects of TiO_2. A method to optimize TiO_2 is applying the metal phthalocyanine dye-sensitized TiO_2 nanorod. Metal phthalocyanine dye sensitizer is capable to enhance the spectral absorption performance of photocatalyzed materials, but also optimize the energy structure of photocatalyzed materials [29–31]. The photo-generated electron–hole recombination of photocatalytic materials can be improved as long as the peripheral groups of metal phthalocyanine dye sensitizers are modified [32, 33]. Moreover, lower-dimensional nanostructure, such as nanorods, nanotubes and nanosheets, has larger specific surface area than nanoparticles. Meanwhile, the dye loading capacity can be enlarged if these kinds of nanostructure expose more active spots [34].

Metal phthalocyanine, as a type of organic dye sensitizer, possesses exceptional thermal and chemical stability. It shows a strong absorption ability in ultraviolet and near infrared area. In addition, its structure is easy to modify.

The recombined material obtained through metal phthalocyanine TiO_2 sensitization can effectively enhance the light absorption performance of TiO_2 [35–37]. The large conjugated structure of metal phthalocyanine helps itself show better energy-level structure and works well to match the energy-level structure of TiO_2. As a result, the problem of wide conduction-valence gap can be overcome. Attaching specific functional groups for metal phthalocyanine can improve the photocatalytic activity of composite materials to some extent. For example, metal phthalocyanine attaches ester functional groups with dioxygen structure as the anchored group, which can boost photo-sensitizer and TiO_2 to connect [38]. The attachment to electronic groups can optimize the energy-level structure of composite materials [39].

In this paper, two types of metal phthalocyanines modified by two varied functional groups (ZnTBPP and ZnTTPP) are synthesized. Besides, TiO_2 nanorods are prepared by taking P25 as titanium through the hydrothermal method. The synthesized metal phthalocyanine is used to sensitize TiO_2 nanoparticles (P25) and TiO_2 nanorods (PN). Then, four types of metal phthalocyanine-sensitized TiO_2 composite photocatalytic materials (ZnTBPP/P25, ZnTTPP/P25, ZnTBPP/PN and ZnTTPP/PN) are obtained. The structure and performance of composite photocatalytic materials are characterized and analyzed. The XRD and SEM are applied to analyze the crystal structure and morphology of composite photocatalytic materials. The UV–Vis diffuse reflectance spectroscopy is adopted to analyze the light absorption performance of composite photocatalytic materials. The fluorescence spectrum is used to study the electron–hole longevity of composite photocatalytic materials. The density-functional theory is utilized to analyze the energy-level structure of composite photocatalytic materials. At last, the photocatalytic degradation of RhB is taken as an example to study the photocatalytic activity of composite photocatalytic materials.

Experimental

Materials and methods

All reagents and solvents are purchased through commercial channels and no further purification is required before use. The ^{1}HNMR of ZnTBPP and ZnTTPP were performed on the spectrometer (Bruker Avance 400). The Rigaku X-ray diffractometer (XRD, R-AXIS RAPID) and field emission scanning electron microscopy (SEM, FEI NOVA NANOSEM 450) are applied to analyze the crystal structure and morphology of photocatalytic materials. Other instrument information is as follows: Fourier-transform infrared spectroscopy (FT-IR, Shimadzu-4800 s); spectro-photometer (UV-2300); UV–Vis diffuse reflectance spectrometer (UV–Vis-DRS, Shimadzu-UV525); fluorescence spectrometer (Hitachi FL-4500); and density-functional theory (DFT, Spartan 08 package).

Synthesis of metal phthalocyanines ZnTBPP and ZnTTPP

The synthetic routes of the metal phthalocyanines are shown in **Scheme S1** (Online Resource). The synthesis routes of ZnTBPP and ZnTTPP. The detailed synthetic procedures are as follows [40, 41]. The chemical structures of ZnTBPP and ZnTTPP are shown in Fig. 1.

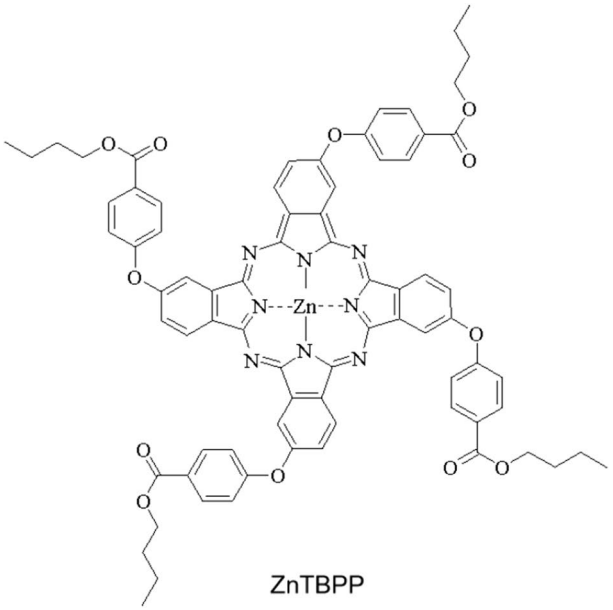

Fig. 1 Chemical structures of ZnTBPP and ZnTTPP

Zn Tetra(butylformate-phenoxy)phthalocyanine (ZnTBPP)

The ZnTBPP was prepared by a two-step method. The first step is to synthesize 4-(3,4-dicyano-phenoxy)-benzoic acid butyl ester (DPB). The butyl p-hydroxybenzoate (2.910 g, 0.015 mol) and K_2CO_3 (2.000 g, 0.014 mol) was added to DMF solution (30 ml). The mixture was slowly heated to 75 °C. The 4-nitrophthalonitrile (2.598 g, 0.015 mol) was added after stirring for 0.5 h with the protection of N_2. The reaction was proceeded at 75 °C for 30 h with the protection of N_2. Finally, mixture was poured into 200 ml ice water and stirred for 0.5 h and the solvent was removed under reduced pressure. A light green crystal of DPB was obtained. The second step is that DPB (1.281 g, 4 mmol) and $(CH_3COO)_2Zn$ (0.219 g, 1 mmol) was added in N-pentanol (40 ml). The mixture was stirred for 0.5 h at 150 °C under N_2 protection. The reaction was proceeded at 150 °C for 24 h with the protection of N_2 after adding DBU (2 ml) as a catalyst. Finally, mixture was poured into methanol solution (50 ml) and the solvent was removed under reduced pressure. Purification by silica gel column chromatography ($CH_2Cl_2/CH_3COOC_2H_5 = 4/1$) afforded ZnTBPP as a green solid.

Yield: 58%. Mp: > 300 °C. ^{1}H-NMR (DMSO-d6, 400 MHz, ppm): $\delta = 8.15$ (d, 4H), 8.05 (m, 8H), 7.93 (d, 4H), 7.55 (m, 4H), 7.29 (m, 8H), 4.28 (t, 8H), 1.72–1.67 (m, 8H), 1.45–1.41 (m, 8H), 0.93 (t, 12H). FT-IR (KBr): v, cm^{-1}, 2931, 2350, 1703, 1600, 1479, 1251,1105, 950, 860, 736. UV–Vis (DMF) λ_{max}/nm, 352, 608, 672.

Zn Tetra(tert-butyl-phenoxy)phthalocyanine (ZnTTPP)

The ZnTTPP was prepared by a two-step method. The first step is to synthesize 4-(4-tert-butyl-phenoxy)-phthalonitrile (BPP). The tert-butylphenol (2.253 g, 0.015 mol) and K_2CO_3 (2.000 g, 0.014 mol) was added to DMF solution (30 ml). The mixture was slowly heated to 75 °C. The 4-nitrophthalonitrile (2.598 g, 0.015 mol) was added after stirring for 0.5 h with the protection of N_2. The reaction was proceeded at 75 °C for 30 h with the protection of N_2. Finally, mixture was poured into 200 ml ice water and stirred for 0.5 h and the solvent was removed under reduced pressure. A brown solid of BPP was obtained. The second step is that BPP (1.104 g, 4 mmol) and $(CH_3COO)_2Zn$ (0.219 g, 1 mmol) was added in N-pentanol (40 ml). The mixture was stirred for 0.5 h at 150 °C under N_2 protection. The reaction was proceeded at 150 °C for 24 h with the protection of N_2 after adding DBU (2 ml) as a catalyst. Finally, mixture was poured into methanol solution (50 ml) and the solvent was removed under reduced pressure. Purification by silica gel column chromatography ($CH_2Cl_2/CH_3COOC_2H_5 = 4/1$) afforded ZnTTPP as a green solid.

Yield: 56%. Mp: > 300 °C. ^{1}H-NMR (DMSO-d6, 400 MHz, ppm): $\delta = 8.07$ (d, 4H), 7.75 (d, 4H), 7.51 (m, 8H), 7.33 (m, 4H), 7.11 (m, 8H), 1.30 (s, 36H). FT-IR(KBr): v, cm^{-1}, 2935, 2350, 1600, 1483, 1240, 1199, 948, 831, 730. UV–Vis (DMF) λ_{max}/nm, 353, 609, 670.

The preparation of TiO_2 nanorods

TiO_2 nanorods are prepared by taking P25 as titanium through the hydrothermal method. 2.0 g of P25 was added to 60 mL NaOH (10 mol/L) under vigorous stirring at room temperature for 4 h. Then, the mixture was transferred into a Teflon-lined stainless steel autoclave and heated to 200 °C kept for 24 h. After cooling to room temperature, the product is washed with distilled water until pH was at around 7. The product is vacuum dried at 80 °C for 3 h. The dried product was added to 60 ml HCl (0.1 mol/L) and stirred for 3 h. Then, the mixture was transferred into a Teflon-lined stainless steel autoclave and heated to 180 °C kept for 24 h. Finally, the TiO_2 nanorods were obtained by vacuum drying for 4 h.

Preparation of composite photocatalytic materials (ZnTBPP/P25, ZnTTPP/P25, ZnTBPP/PN and ZnTTPP/PN)

Prepared two metal phthalocyanine-sensitized P25 composite photocatalytic materials (ZnTBPP/P25, ZnTTPP/P25). Metal phthalocyanine 0.01 g (ZnTBPP, ZnTTPP) and P25 (1.00 g) are dissolved in DMF (10 ml) and absolute ethanol (20 ml). The mixture was stirred at room temperature for 3 h. Then, the mixture was transferred into a Teflon-lined stainless steel autoclave and heated to 120 °C kept for 48 h. Finally, the products were obtained by vacuum drying at 80 °C for 4 h. The preparation of ZnTBPP/PN and ZnTTPP/PN is the same as ZnTBPP/P25 and ZnTTPP/P25, only P25 needs to be replaced with TiO_2 nanorod.

By measuring the UV–visible light absorbance of the solution before and after adding P25 and TiO_2 nanorods, the loading amount of the metal phthalocyanine on the photocatalytic material was calculated.

Photocatalytic degradation

The 15 mg of photocatalyst (P25, PN, ZnTBPP/P25, ZnTTPP/P25, ZnTBPP/PN and ZnTTPP/PN) was added to RhB (50 ml, 5×10^{-5} mol/L). The mixture was stirred in the dark for 0.5 h. Then, the mixture is transferred to the sunlight simulator and continues to react for 1 h with 4 mL of the suspension suction every 6 min. The absorbance of RhB after high-speed centrifugation is measured by UV–Vis spectro-photometer. The photocatalytic activity of each photocatalytic material can be obtained by the variety of RhB UV–Vis absorbance.

Results and discussion

XRD analysis

The XRD measurement and analysis on P25, PN and composite photocatalytic materials are conducted. As shown in Fig. 2, the peak values at 23.2°, 37.9°, 48.1°,

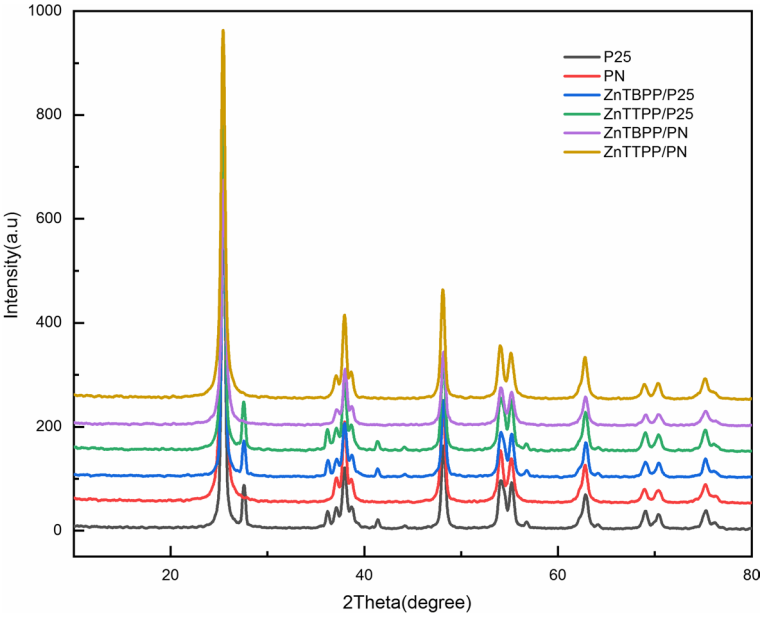

Fig. 2 XRD patterns of P25, PN and composite photocatalytic materials

54.0°, 55.2°, 62.8°, 69.0°, 70.4° and 75.2° clearly represent the formation of anatase crystals. The XRD peak broadening of anatase crystals shows that P25, PN and composite photocatalytic materials are all nanoscale. Moreover, the metal phthalocyanine loading has no impact on the crystal structure of composite photocatalytic materials as metal phthalocyanine trace loads.

Analysis

The morphology and structure of P25, PN and composite photocatalytic materials are analyzed through SEM. As shown in Fig. 3, the formation of nanorod structure can be seen by comparing the SEM graphs of P25 and PN. Compared with easily aggregated nanoparticles, nanorod structure has larger specific surface area, which is conducive to metal phthalocyanine loading. The SEM graphs of four composite photocatalytic materials are observed and analyzed. It is found that the morphology and structure show no obvious change. Only the appearance turns rougher. The loading amount of metal phthalocyanine is calculated through analyzing the UV–visible absorption spectra of the preloaded and loaded solutions. The calculation process and results are shown in Table S1 (Online Resource). In terms of the load capacity, ZnTBPP/PN > ZnTTPP/PN > ZnTBPP/P25 > ZnTTPP/P25. The reason is that the larger specific surface area of nanorods helps metal phthalocyanine loading. Furthermore, compared with ZnTTPP, ZnTBPP has four ester groups peripherally, which boosts the combination between metal phthalocyanine and TiO_2. Greater

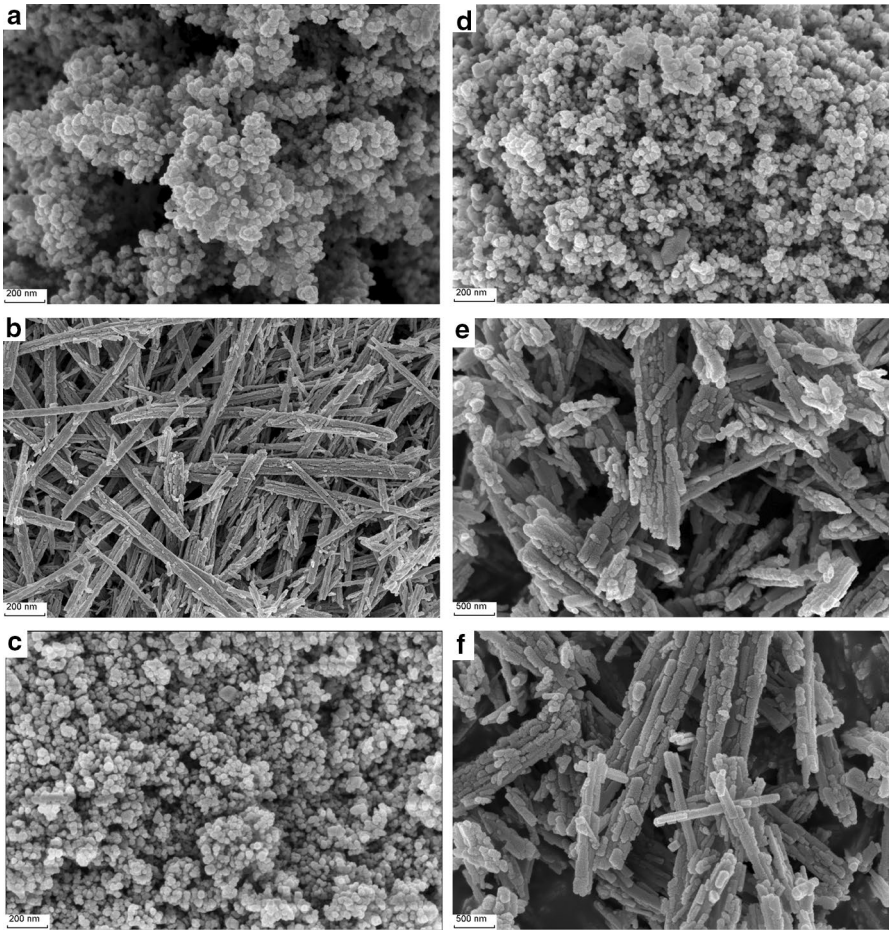

Fig. 3 SEM **a–f** images of P25, PN, ZnTBPP/P25, ZnTTPP/P25, ZnTBPP/PN and ZnTTPP/PN

loading means more exceptional photocatalytic performance, which can be reflected in the final photocatalytic degradation of RhB.

FT-IR analysis

The Fourier-transform infrared spectroscopy is utilized to analyze P25, PN and composite photocatalytic materials. The results are shown in Fig. 4. Through the spectra analysis, it shows that the characteristic absorption peaks of hydroxyl groups at 3420 cm^{-1} and 1630 cm^{-1} appear for P25 and PN. It indicates that hydroxyl groups exist on the surface of TiO_2. Furthermore, metal phthalocyanine appears at the C-H stretching vibration characteristic peak at 2935 cm^{-1} and at the ether symmetric stretching vibration characteristic peak at 1240 cm^{-1}. It means that metal phthalocyanine successfully loads on P25 and PN.

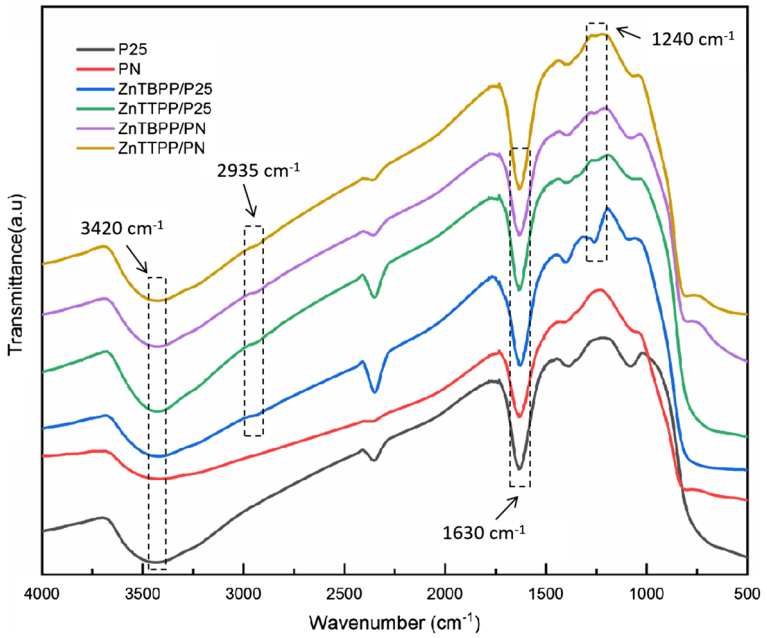

Fig. 4 FT-IR spectra of P25, PN and composite photocatalytic materials

UV–Vis-DRS analysis

The UV–Vis diffuse reflectance spectroscopy is used to study the spectral absorption performance of P25, PN and composite photocatalytic materials in the range of 200 nm to 800 nm. As shown in Fig. 5, P25 and PN have light absorption only within 400 nm. But the two absorb at 550 nm-750 nm for the four composite photocatalytic materials. This indicates that metal phthalocyanine loading can extend the photoresponse range of photocatalytic materials. Moreover, the characteristic absorption peak of phthalocyanine appears at 670 nm for all four composite photocatalytic materials. This indicates that metal phthalocyanine completely loads on TiO_2. Hence, the metal phthalocyanine loading enlarges the light response range of TiO_2 from ultraviolet area to ultraviolet–visible area, and enhances the light absorption performance of composite photocatalytic materials. As a result, the photocatalytic performance of composite photocatalytic materials is strengthened.

BET analysis

The N_2 adsorption–desorption isotherm is an analytical method used to study the specific surface area of a substance. It can be seen from Figure S6 (Online Resource) that all six photocatalytic materials exhibit typical IV isotherm. The specific surface areas of P25, PN, ZnTBPP/P25, ZnTTPP/P25, ZnTBPP/PN and ZnTTPP/PN are 48.44 cm^{-3}/g, 80.77 cm^{-3}/g, 46.95 cm^{-3}/g, 47.44 cm^{-3}/g, 76.90 cm^{-3}/g and

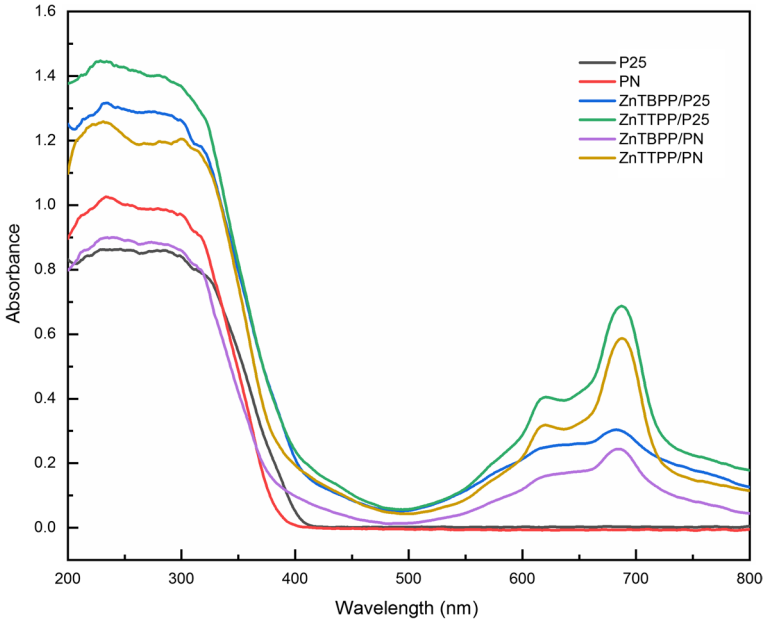

Fig. 5 UV–Vis-DRS spectra of P25, PN and composite photocatalytic materials

77.11 cm^{-3}/g, respectively. The specific surface area of PN is significantly increased compared with P25. A larger specific surface area is conducive to the adsorption of metal phthalocyanine, which is verified in the adsorption capacity test results. In addition, compared with P25 and PN, the sensitization of metal phthalocyanine leads to a decrease in the specific surface area of the composite photocatalytic material.

Fluorescence spectra analysis

The fluorescence spectra of P25, PN and composite photocatalytic materials are used to conduct the characteristic analysis to study the impacts of metal phthalocyanine loading on the electron–hole longevity of composite photocatalytic materials. From Fig. 6, it can be seen that the four composite photocatalytic materials all perform less strongly in absorption peaks. Electron–holes can be generated in photogenerated materials under the light stimulation. Some of electron–holes are applied to conduct the redox reaction for degrading organic pollutants, while the other part are utilized to undergo the electron–hole recombination. The energy generated by electron–hole recombination can be released in the form of light. Therefore, the low-intensity fluorescence absorption peak represents the low-degree electron–hole recombination. The results show that the metal phthalocyanine loading can weaken the electron–hole recombination of photocatalyzed materials to a certain extent. Thus, the photocatalyzed performance of composite photocatalyzed materials is

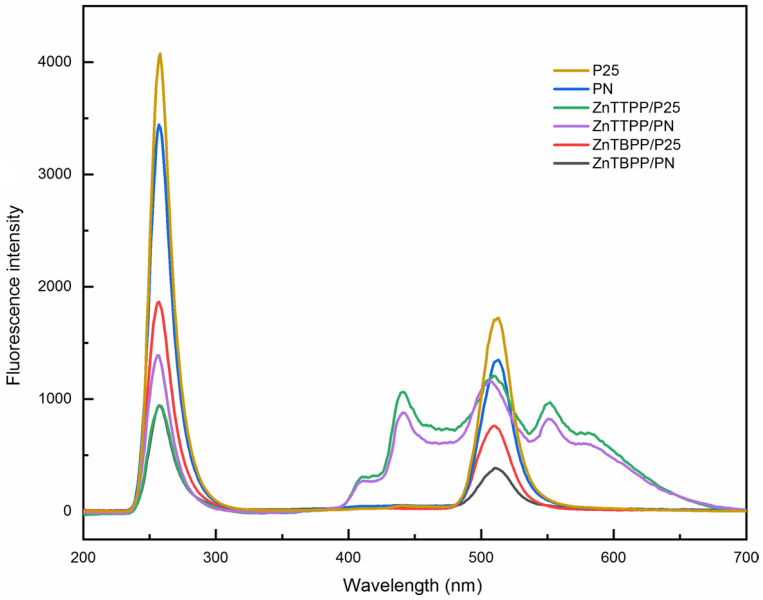

Fig. 6 Fluorescence spectra of P25, PN and composite photocatalytic materials

stronger than that of P25 and PN. Moreover, comparing the fluorescence spectra of ZnTBPP and ZnTTPP loaded composite photocatalytic materials, the absorption intensities of ZnTTPP/P25 and ZnTTPP/PN are higher than those of ZnTBPP/P25 and ZnTBPP/PN. The reason is that the electronic group tert-butyl on the periphery of ZnTTPP can increase the fluorescence absorption. In comparison, the electron-withdrawing group N-butyl formate on the periphery of ZnTBPP can scale down the fluorescence absorption.

Density-functional theory analysis

It is to study the role of metal phthalocyanine loading on the energy-level structure of composite photocatalytic materials and the electron transfer in composite photocatalytic materials during the photocatalysis. Density-functional theory (DFT) is deployed to do the quantum chemistry calculation of ZnTBPP and ZnTTPP. Figure 7. The HOMO, LUMO and conduction-valence gap Eg of ZnTBPP and ZnTTPP are calculated by DFT. As shown in Fig. 8, it can be seen that the conduction-valence gaps of ZnTBPP and ZnTTPP are 2.16 eV and 2.13 eV, respectively. Both values are smaller than that of TiO_2 (3.2 eV). The results indicate that ZnTBPP and ZnTTPP can conduct electronic transition under sunlight prior to TiO_2. The LUMO values of ZnTBPP and ZnTTPP are −2.97 eV and −2.66 eV, respectively, which are higher than that of TiO2 (−4.0 eV). The results indicate that the electrons produced by ZnTBPP and ZnTTPP transition can be effectively transferred to TiO_2 conduction band.

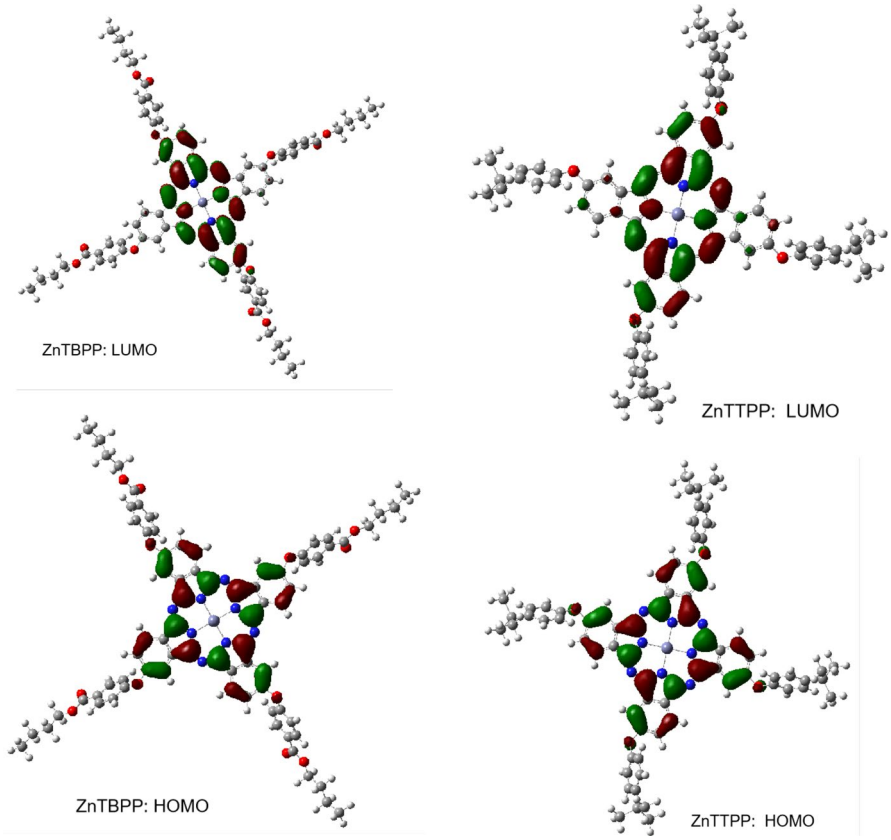

Fig. 7 The HOMO and LUMO energy-level structure of ZnTBPP and ZnTTPP

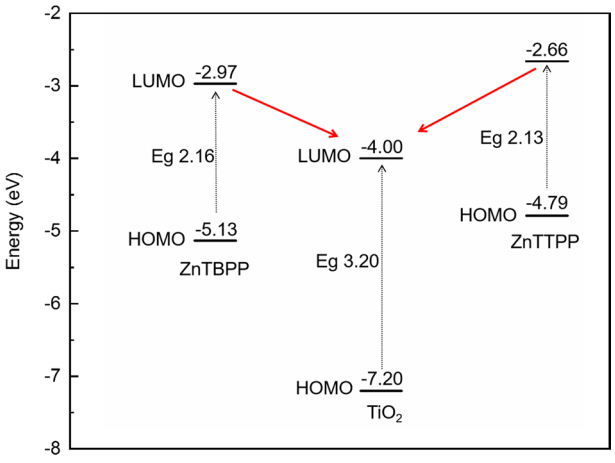

Fig. 8 The energy-level structure diagrams of TiO_2, ZnTBPP and ZnTTPP

The electron transfer on composite photocatalytic materials during the photocatalytic process is studied and analyzed. Then is shown in Fig. 9. The sunlight irradiation first induces the metal phthalocyanine to generate electrons through the electronic transfer. Then, the electrons are transferred to TiO_2 conduction band for reacting with O_2 in the air. HOO· and OH· with a high activity are generated, which continue to react and trigger the degradation of organic pollutants.

Photocatalytic activity

The photocatalytic activity of P25, PN and composite photocatalytic materials is analyzed by the photocatalytic degradation of RhB under the sunlight simulator. Figure 10 shows, It displays the photocatalytic efficiency of each photocatalytic material in the comparison of blank experiments. The results are in line with the expected ones: ZnTBPP/PN > ZnTTPP/PN > ZnTBPP/P25 > ZnTTPP/P25 > PN > P25. In general, the photocatalytic activities of the four composite photocatalytic materials are stronger than those of ordinary TiO_2. Based on the analysis of photocatalytic process, the reasons are summarized in three aspects. Firstly, metal phthalocyanine loading improves the light absorption performance of photocatalyzed materials. Secondly, the existence of metal phthalocyanine weakens the electron–hole recombination of photocatalyzed materials. Finally, the energy-level structure of metal phthalocyanine matches with TiO_2, which can optimize the energy-level structure of composite photocatalyzed materials to some extent.

Moreover, the photocatalytic activities of ZnTBPP/PN, ZnTTPP/PN and PN with ZnTBPP/P25, ZnTTPP/P25 and P25 are compared. It can be found that the nanorod structure demonstrates exceptional performance compared with nanoparticles. This is attributed to the large specific surface area of nanorod structure, which can expose more active spots but also promote metal phthalocyanine loading. Comparing ZnTBPP/PN and ZnTTPP/PN, ZnTBPP/P25 and ZnTTPP/P25, it is found that the photocatalytic activity of loaded ZnTBPP is stronger than that of ZnTTPP. This is probably because the existence of ester groups in ZnTBPP enhances the electron transfer between metal gold phthalocyanine molecules and TiO_2.

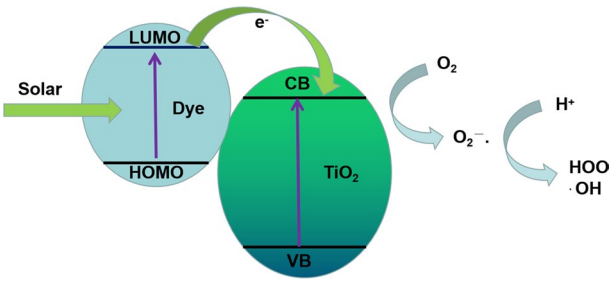

Fig. 9 The diagram of photocatalytic process

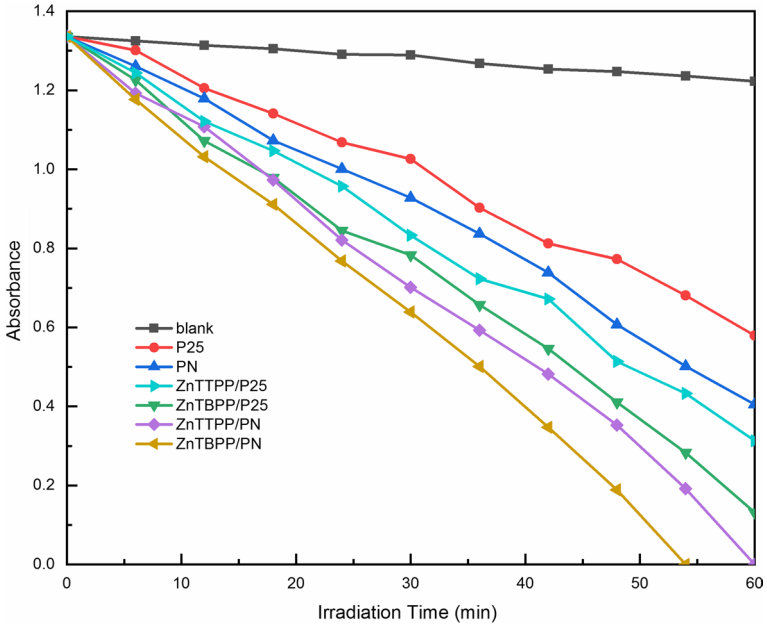

Fig. 10 The photodegradation of RhB using different photocatalysts materials

Conclusions

In summary, the photocatalytic activity of the four composite photocatalytic materials is stronger than that of TiO_2. It shows that metal phthalocyanine-sensitized TiO_2 nanorods can effectively improve the defects of TiO_2 and enhance its photocatalytic activity. In the process of photocatalytic degradation of organics, the loading of metal phthalocyanine can enhance the light absorption performance of the photocatalytic material, optimize the energy-level structure of the photocatalytic material, and reduce the electron–hole recombination, thereby enhancing the photocatalytic activity of the photocatalytic material. In particular, ZnTBPP/PN has the strongest photocatalytic activity among all photocatalytic materials. This is because PN has a larger specific surface area than P25, which can increase the loading of metal phthalocyanine and expose more active sites. In addition, compared with ZnTTPP, the presence of ester groups in ZnTBPP enhances the electron transfer between metal phthalocyanine molecules and TiO_2.Therefore, ZnTBPP/PN has the highest photocatalytic activity.

Acknowledgements This work was supported by the Foundation of Shanxi Province, China (Grant No. 2015011011), and the Research Project Supported by Shanxi Scholarship Council of China (Grant No. 2015-078)

Compliance with ethical standards

Conflict of interest There are no conflicts to declare.

References

1. N. Ahmadpoura, M.H. Sayadia, S. Sobhanib, M. Hajiani, J. Environ. Manage. **271**, 110964 (2020)
2. R.S. Kumar, H. Kim, N. Mergu, Y.A. Son, Res. Chem. Intermed. **46**, 313 (2020)
3. W.J. Sun, J. Li, X.F. Lu, F.X. Zhang, Res. Chem. Intermed. **39**, 1447 (2013)
4. X.J. Yua, H.R. Qiua, B. Wangc, Q.N. Menga, S.D. Sunb, K. Zhao, Y.f. Tanga. J. Alloys Compd. **839**, 155597 (2020)
5. H. Park, H. Kim, G. Moon, W. Choi, Energy Environ. Sci. **9**, 411 (2016)
6. F.Y. Chen, W.J. An, L. Liu, Y.H. Liang, W.Q. Cui, Appl. Catal. B **217**, 65 (2017)
7. M. Muuronen, S.M. Parker, E. Berardo, A. Le, M.A. Zwijnenburg, F. Furche, Chem. Sci. **8**, 2179 (2017)
8. J. Schneider, M. Matsuoka, M. Takeuchi, J.L. Zhang, Y. Horiuchi, M. Anpo, D.W. Bahnemann, Chem. Rev. **114**, 9919 (2014)
9. Y. Ma, X.L. Wang, Y.S. Jia, X.B. Chen, H.X. Han, C. Li, Chem. Rev. **114**, 9987 (2014)
10. D. Laishram, K.P. Shejale, R. Gupta, R.K. Sharma, Mater. Lett. **231**, 225 (2018)
11. P. Wang, J. Wang, T. Ming, X. Wang, H. Yu, Y. Wang, M. Lei, A.C.S. Appl, Mater. Interf. **5**, 2924 (2013)
12. J.W. Kim, H.S. Kim, K.H. Yu, A. Fujishima, Y.S. Kim, B. Kor, Chem. Soc. **31**, 2849 (2010)
13. O.A. Osin, T.Y. Yu, X.M. Cai, Y. Jiang, G.T. Peng, X.M. Cheng, R.B. Li, Y. Qin, S.J. Lin, Front. Chem. **6**, 192 (2018)
14. X.Y. Zhang, J.L. Huang, Z.W. Kang, D.P. Yang, R. Luque, Mol. Catal. **484**, 110786 (2020)
15. Y. Zhao, N. Hoivik, K. Wang, Nano Energy. **30**, 728 (2016)
16. A. Eshaghi, H. Moradi, Adv. Powder Technol. **29**, 1879 (2018)
17. F. Bashiri, M. Khezri, R.R. Kalantary, B. Kakavandi, J. Mol. Liq. **314**, 113608 (2020)
18. M. Kermani, B. Kakavandi, M. Farzadkia, A. Esrafili, S.F. Jokandan, A. Shahsavani, J. Clean. Prod. **192**, 597 (2018)
19. D.R. Zhang, H.L. Liu, S.Y. Han, W.X. Piao, J. Ind. Eng. Chem. **19**, 1838 (2013)
20. K. Zhao, Z.M. Wu, R. Tang, Y.D. Jiang, Y.X. Lu, Res. Chem. Intermed. **41**, 4405 (2015)
21. A. Bokare, M. Pai, A.A. Athawale, Sol. Energy. **91**, 111 (2013)
22. A.Q. Deng, Y.F. Zhu, Res. Chem. Intermed. **44**, 4227 (2018)
23. J. Huang, X. Guo, B. Wang, J. Spectrosc. **8**, 681850 (2015)
24. H. Jafari, S. Afshar, O. Zabihi, M. Naebe, Res. Chem. Intermed. **42**, 2963 (2016)
25. W. Zhang, C. Wang, X. Liu, J. Li, J. Mater. Res. **32**, 14 (2017)
26. M.A. Dil, A. Haghighatzadeh, B. Mazinani, Bull. Mater. Sci. **42**, 248 (2019)
27. D.Y. Zhou, W. Liang, W.G. Zhang, Y.M. Liu, F.Q. Yang, J. Nanosci. Nanotechnol. **18**, 4397 (2018)
28. S.Z. Kang, Z.Z. Xu, Y.X. Song, J. Mu, J. Dispersion Sci. Technol. **27**, 857 (2006)
29. M.Y. Zhang, C.L. Shao, Z.C. Guo, Z.Y. Zhang, J.B. Mu, P. Zhang, T.P. Cao, Y.C. Liu, A.C.S. Appl, Mater. Interfaces. **3**, 2573 (2011)
30. H. Ding, M.K. Ram, C. Nicolini, J. Nanosci. Nanotechnol. **1**, 207 (2001)
31. L.Y. Mo, H.T. Zheng, Haitao. J. Alloys Compd. **788**, 1162 (2019)
32. W.Q. Wei, D. Liu, Z. Wei, Y.F. Zhu, ACS Catal. **7**, 652 (2017)
33. W.Q. Cui, J. He, H. Wang, J.S. Hu, L. Li, Y.H. Liang, Appl. Catal. B **232**, 232 (2018)
34. L.T. Tseng, X. Luo, T.T. Tan, S.A. Li, J.B. Yi, Nanoscale Res. Lett. **9**, 673 (2014)
35. L. Lapok, G. Schnurpfeil, R. Gerdes, S.M. Gorun, O. Suvorova, D. Woehrle, J. Porphyrins Phthalocyanines. **13**, 346 (2009)
36. L. Giribabu, R.K. Kanaparthi, V. Velkannan, Chem. Rec. **12**, 306 (2012)
37. M.V. Martinez-Diaz, M. Ince, T. Torres, Monatsh. Chem. **142**, 699 (2011)
38. L. Zhang, J.M. Cole, A.C.S. Appl, Mater. Interfaces. **7**, 60439 (2015)
39. S.L. Wu, H.P. Lu, H.T. Yu, S.H. Chuang, C.L. Chiu, C.W. Lee, E.W.G. Diau, C.Y. Yeh, Energy Environ. Sci. **3**, 949 (2010)
40. M.L. Han, X.J. Zhang, X.X. Zhang, C.Q. Liao, B.Q. Zhu, Q.L. Li, Polyhedron **85**, 864 (2015)
41. X.J. Zhang, X.L. Pei, C.Q. Liao, L. Zou, Res. Chem. Intermed. **43**, 2737 (2017)